Biomedical Physics &
Engineering Express

Endorsed by IPEM Institute of Physics and Engineering in Medicine
PURPOSE-LED PUBLISHING™

PAPER • **OPEN ACCESS**

Effect of tissue viscoelasticity on delivered mechanical power in a physical respiratory system model: distinguishing between airway and tissue resistance

To cite this article: Simon Walzel and Karel Roubik 2025 *Biomed. Phys. Eng. Express* **11** 015026

Biomedical Physics & Engineering Express

PAPER

Effect of tissue viscoelasticity on delivered mechanical power in a physical respiratory system model: distinguishing between airway and tissue resistance

Simon Walzel and Karel Roubik

Department of Biomedical Technology, Faculty of Biomedical Engineering, Czech Technical University in Prague, Kladno, Czech Republic

E-mail: walzesim@fbmi.cvut.cz

Keywords: viscoelasticity, tissue resistance, physical respiratory system model, mechanical ventilation, mechanical power

Supplementary material for this article is available online

OPEN ACCESS

RECEIVED
25 September 2024

REVISED
17 November 2024

ACCEPTED FOR PUBLICATION
26 November 2024

PUBLISHED
4 December 2024

Abstract

Understanding the mechanics of the respiratory system is crucial for optimizing ventilator settings and ensuring patient safety. While simple models of the respiratory system typically consider only flow resistance and lung compliance, lung tissue resistance is usually neglected. This study investigated the effect of lung tissue viscoelasticity on delivered mechanical power in a physical model of the respiratory system and the possibility of distinguishing tissue resistance from airway resistance using proximal pressure measured at the airway opening. Three different configurations of a passive physical model of the respiratory system representing different mechanical properties (Tissue resistance model, Airway resistance model, and No-resistance model) were tested. The same volume-controlled ventilation and parameters were set for each configuration, with only the inspiratory flow rates being adjusted. Pressure and flow were measured with a Datex-Ohmeda S/5 vital signs monitor (Datex-Ohmeda, Madison, WI, USA). Tissue resistance was intentionally tuned so that peak pressures and delivered mechanical energy measured at airway opening were similar in Tissue and Airway Resistance models. However, measurements inside the artificial lung revealed significant differences, with Tissue resistance model yielding up to 20% higher values for delivered mechanical energy. The results indicate the need to revise current methods of calculating mechanical power delivery, which do not distinguish between tissue resistance and airway flow resistance, making it difficult to evaluate and interpret the significance of mechanical power delivery in terms of lung ventilation protectivity.

1. Introduction

Respiratory system can be described as a pneumatic circuit, simply defined by resistance (R) and compliance (C). However, simple linear models consisting of only R and C, which are crucial for understanding the fundamentals of mechanical behavior, may have limited validity due to the nonlinearities, inhomogeneities, and structural complexity that characterize the entire respiratory system. Numerous studies have been conducted to develop reliable physical models (Höhne *et al* 2021, Pasteka *et al* 2019, Wenzel *et al* 2020) and computer models (Wall *et al* 2010, Roth *et al* 2017, Ionescu *et al* 2009) of the respiratory system, e.g., to outline some of the mechanical properties of the respiratory system or to compare different ventilation modes.

The total resistance of the respiratory system is determined not only by the flow resistance in the airways but also by the resistance of the lung tissue (Bates 2009). Tissue resistance can be attributed to several factors, including viscoelasticity (Similowski *et al* 1989, Suki *et al* 1994), nonlinear viscoelasticity (Birzle and Wall 2019, Goswami *et al* 2022), fractional viscoelasticity (Dai *et al* 2015), poroelasticity (Berger *et al* 2016, Concha and Hurtado 2020), pendelluft (Santini *et al* 2019) or, for example, surface tension (Escolar and Escolar 2004). Then, the changes in total resistance can be caused, for example, by an obstructed endotracheal tube, an airway narrowing or the tissue resistance changes (Guerin and Richard 2007). The method for measuring tissue resistance involves maintaining a constant volume during inspiratory occlusion and measuring the

pressure. When inspiratory flow is stopped, the pressure drops rapidly from its peak value to a lower value P_1, which represents the alveolar pressure. This rapid drop in pressure is caused by flow resistance, both artificial and anatomical. During inspiratory occlusion, a slower decrease in pressure to the plateau pressure (P_{plat}) value is observed (Mezidi *et al* 2017). This additional pressure decrease is mainly caused by the stress relaxation in the parenchyma, usually assigned to viscoelasticity (Ganzert *et al* 2009, Protti *et al* 2016, Santini *et al* 2019). Under dynamic conditions, P_1 reflects alveolar pressure more accurately than P_{plat} and therefore, it can be used to predict the actual pressures acting on the lung parenchyma (Santini *et al* 2019). The value of P_{plat} is used to calculate the total resistance and compliance of the respiratory system but it has been found that P_{plat} readings taken at 0.5 s and 5 s of inspiratory occlusion produce significantly different results due to the lung tissue viscoelasticity (Barberis *et al* 2003).

Furthermore, higher inspiratory flow rates have been found to require more pressure to inflate the lungs to a given volume than lower inspiratory flow rates (Otis *et al* 1956), and more recently, higher pressures resulting from higher flow rates have been found to be associated with the development of ventilator-induced lung injury (VILI), indicating the effect of viscoelasticity (Protti *et al* 2016). These findings are also supported by the studies of Maeda *et al* (2004) and Santini *et al* (2019), which suggest that when tidal volume is delivered at a higher peak flow rate, gas exchange and respiratory mechanics are impaired, and pulmonary histology appears to be more pronounced than when tidal volume is delivered at a lower peak flow rate. Gattinoni *et al* (2017) suggested that the effect of inspiratory flow and tissue resistance on the protectivity of lung ventilation needs further clarification.

Tidal volume, pressure, and flow are components of the energy load that contribute to the amount of mechanical power delivered to the lungs and it was recently suggested that mechanical power is also a strong predictor of VILI risk (Cressoni *et al* 2016, Silva *et al* 2019, Marini *et al* 2023). The mechanical energy delivered by the lung ventilator to the lungs can be calculated from the pressure-volume (PV) loop as the area enclosed beneath the inspiratory curve of the airway pressure against the inspired volume, expressed in Joules (Marini *et al* 1986). This is usually referred to as the geometric method. Simply multiplying the mechanical energy delivered during one respiratory cycle by the respiratory rate per minute gives the value of the delivered mechanical power. Various simplifications of mechanical power calculations have been proposed in the last years to facilitate calculations in clinical environments (Gattinoni *et al* 2016, Giosa *et al* 2019, Marini and Jaber 2016, Chi *et al* 2021).

However, airway flow resistance is not explicitly distinguished from tissue resistance in any of these methods of calculating mechanical power delivery to the lungs. Therefore, the P_{plat} used in the calculations may not accurately quantify the forces and injurious energy that cause damage. The small pressure difference between P_1 and P_{plat}, which probably corresponds to viscoelastic losses (Guerin and Richard 2007, Protti *et al* 2016, Gattinoni *et al* 2017, Marini *et al* 2023), is buried in what is usually clinically assigned to the difference between peak pressure and P_{plat}, which caregivers use to calculate airway flow resistance. This hidden pressure difference involves unmeasured energy spent on viscoelastic losses and potentially on the direct infliction of damage by microfractures of extracellular matrix elements (Marini *et al* 2023).

The aim of this study was to develop a passive physical model of the respiratory system that simulates lung tissue viscoelasticity and airway flow resistance, and to use this model to determine whether it is possible to distinguish tissue resistance from airway flow resistance using proximal pressure measured at the airway opening.

2. Methods

2.1. Viscoelastic respiratory system model

A special apparatus comprising a passive bellow-based Adult Lung Simulator (Michigan Instruments, Kentwood, MI, USA), a 20 ml borosilicate glass syringe (Socorex, Ecublens, Switzerland), and a throttle valve was assembled. The throttle valve was connected to the Luer adapter of the syringe to regulate the airflow into the syringe, thereby creating a tissue resistance. The glass syringe with the throttle valve was mounted parallel to the one artificial bellow lung of the Simulator using custom made 3D printed parts and fixtures, as shown in figure 1. The syringe serves as a mechanical damper with minimal frictional resistance, thanks to the low friction coefficient of the borosilicate glass. Supplementary material 1 provides details on the testing method and the results of the negligible impact of frictional resistance on measured pressure and flow.

The mechanical properties of the viscoelastic respiratory system model are thus determined by a linear compliance C_L (a spring as an integral part of the Simulator), representing the static elastic properties, and a compliance C_t with a dashpot resistance R_t (the glass syringe with the throttle valve), forming the so-called Maxwell body (a type of a mechanical rheological model) and representing the viscoelastic properties. The model represents a single homogenous physical compartment, but still has two degrees of freedom, as described by Bates (Bates 2009). The magnitude of the pressure in the respiratory system model at any moment in time is defined by two quantities—the volume of gas in the artificial lung and the flow to or from the syringe, i.e., the actual pressure in the syringe chamber. During the inspiratory phase, negative pressure is created and during exhalation, on the contrary, overpressure is created inside the syringe chamber.

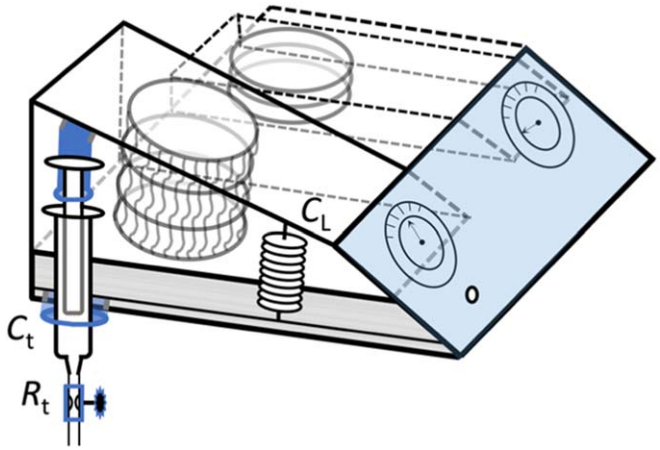

Figure 1. The Adult Lung Simulator with the glass syringe and the throttle valve mounted parallel to the one artificial bellow lung representing the tissue resistance of the viscoelastic respiratory system model. The spring represents the static elastic properties of the viscoelastic respiratory system model.

2.2. Testing

Three different configurations of a passive physical respiratory system model representing different mechanical properties were tested:

1. Tissue resistance model: viscoelastic respiratory system model with tissue resistance ($R_t + C_t$) and with no airway resistance (R_{aw}),
2. Airway resistance model: respiratory system model with linear airway resistance (R_{aw}) of 5 $cmH_2O{\cdot}s{\cdot}L^{-1}$ (Model 7100R, Hans Rudolph Inc., Shawnee, KS, USA) and with no tissue resistance ($R_t + C_t$),
3. No-resistance model: respiratory system model with no airway resistance (R_{aw}) and with no tissue resistance ($R_t + C_t$).

The linear compliance (C_L) of the artificial lung was set at 30 $ml{\cdot}cmH_2O^{-1}$ for all the configurations.

To determine whether tissue resistance can be distinguished from airway resistance by proximal pressure measured at the airway opening, Airway resistance model with R_{aw} of 5 $cmH_2O{\cdot}s{\cdot}L^{-1}$ served as a reference model. The airflow resistance of the throttle valve in Tissue resistance model was tuned to achieve the same maximum airway pressure measured at the airway opening as in Airway resistance model.

Ventilation was provided by a Veolar lung ventilator (Hamilton Medical, Bonaduz, Switzerland), on which volume-controlled ventilation was set with the following parameters: tidal volume $Vt = 1000$ ml, constant flow during inspiration, positive end-expiratory pressure ($PEEP$) = 5 cmH_2O, inspiratory to expiratory time ratio ($I{:}E$) = 1:1, inspiratory occlusion = 20%, and respiratory rate (RR) = 6, 12 or 18 min^{-1}, corresponding to inspiratory flow rates (Q_{insp}) of approximately 20, 40 and 60 $l{\cdot}min^{-1}$. The same ventilation parameters were set for each configuration.

Airway pressure (P_{aw}) and flow (Q) were measured using a D-Lite spirometric sensor of the Datex-Ohmeda S/5 vital signs monitor (Datex-Ohmeda, Madison, WI, USA). Due to the lack of an additional gas pressure port on the monitor, the pressure inside the artificial lung (P_L) was measured using the haemodynamic module E-PSMP, which recorded the pressure in millimeters of mercury (mmHg). The measured pressure was then converted from mmHg to cmH_2O. The sampling rate for P_{aw}, Q and P_L was set to 100 Hz. The complete measuring system is shown in figure 2.

2.3. Data processing and statistical analysis

The measured pressure and flow curves from five representative respiratory cycles for different respiratory system model configurations and different respiratory rates were averaged and further processed. Flow rates were converted to delivered tidal volumes over time.

The averaged curves of P_{aw}, Q and P_L and the averaged curves of the dependence of P_{aw} and P_L on the delivered volume for each respiratory rate and configuration were then plotted on graphs. The standard deviations were calculated but were too small to be shown in the graphs.

To mathematically compare the Tissue resistance model with Airway resistance model, the mechanical energy delivered during the inspiratory phase of the respiratory cycle was calculated using a formula representing the geometric method (Marini *et al* 1986, Gattinoni *et al* 2016), where numerical integration was used for the calculation:

$$E = \frac{0.098}{1000}\cdot\sum_i [((P_i + P_{i+1}) - 2{\cdot}PEEP){\cdot}(V_{i+1} - V_i){\cdot}\frac{1}{2}], \quad (1)$$

where E corresponds to the delivered mechanical energy during the inspiratory phase of the respiratory

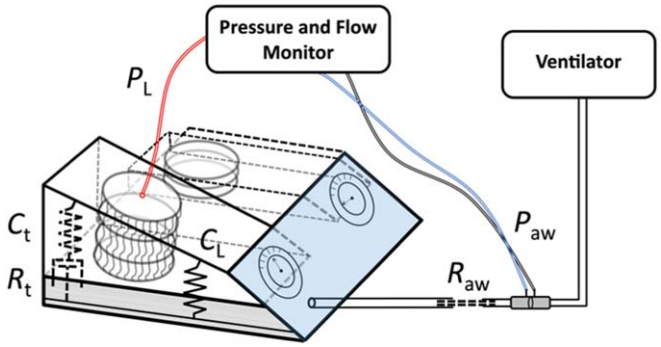

Figure 2. A scheme of the measuring system consisting of a lung ventilator, flow and pressure monitor and configurations of the passive physical respiratory system model representing different mechanical properties. The components representing the dynamic viscous ($R_t + C_t$) and the static elastic (C_L) properties are replaced by the symbols for mechanical rheological models. The connection or disconnection of R_{aw}, R_t or C_t was determined by the tested configuration.

cycle in J, *P* represents the measured pressure at a given time in cmH_2O, *PEEP* is the positive end-expiratory pressure in cmH_2O, *V* is the measured volume at a given time in mL and *i* denotes the number of samples in the inspiratory phase.

The calculation was done using both P_{aw} and P_L in order to compare the values of the delivered mechanical energy measured at the airway opening of the respiratory system model (E_{aw}) and inside the artificial lung (E_L) for all configurations.

3. Results

Connecting the glass syringe with the tuned airflow resistance of the throttle valve in parallel to the artificial lung of the Simulator (Tissue resistance model) resulted in a gradual increase in the measured peak pressures of both P_{aw} and P_L as Q_{insp} increased from 20 $l{\cdot}min^{-1}$ to 60 $l{\cdot}min^{-1}$.

As intended, the P_{aw} curves during the inspiratory phase and the peak P_{aw} overlapped in Tissue resistance model and Airway resistance model. The peak P_{aw} reached approximately 36 cmH_2O for Q_{insp} of 20 $l{\cdot}min^{-1}$ (RR = 6 min^{-1}) and 42 cmH_2O for Q_{insp} of 60 $l{\cdot}min^{-1}$ (RR = 18 min^{-1}) in both Tissue resistance model and Airway resistance model as shown in figure 3. In contrast, P_L curves overlapped during the inspiratory phase in Airway resistance model and No-resistance model. During the inspiratory occlusion, an exponential decrease from the maximum P_{aw} and P_L to P_{plat} was apparent only in Tissue resistance model.

In the expiratory phase of the respiratory cycle, the fastest slope of the pressure decrease occurred in Tissue resistance model, however, the slope decreased towards the end of the expiratory phase and the fastest complete pressure decrease to *PEEP* pressure was observed in No-resistance model.

A detailed analysis of the inspiratory phase showed that the peak P_{aw} did not differ significantly between Tissue resistance and Airway resistance models, as intended, but when looking at the peak P_L, the differences between these models were significant and increased with Q_{insp} (on average 1.6–3.3 cmH_2O according to Q_{insp}), as illustrated in figure 4. During the inspiratory occlusion, in Airway resistance model, P_{aw} rapidly dropped to P_{plat} value that remained constant throughout the inspiratory occlusion. In Tissue resistance model, the pressure exponentially decreased, and the values approached the values measured in Airway resistance model and No-resistance model. Only at RR = 18 min^{-1}, the inspiratory occlusion was too short, lasting about 0.8 s, and did not result in a complete decrease to P_{plat}.

The *PV* loops for P_{aw} in the inspiratory phase in Tissue resistance and Airway resistance models shifted from the loop of No-resistance model with increasing Q_{insp}, reaching higher peak pressures, as illustrated in figure 5. There was no significant difference between the Tissue resistance and Airway resistance models in the inspiratory phase.

However, the results for *PV* loops for P_L were different. As Q_{insp} increased, the loop in the inspiratory phase in Tissue resistance model shifted from the loops of Airway resistance and No-resistance models. Additionally, there was no difference in the inspiratory phase between Airway resistance and No-resistance models.

Table 1 shows that there were no major differences in E_{aw}, calculated from P_{aw}, between Tissue resistance model and Airway resistance model for any respiratory rate (2.08 J versus 2.16 J, 1.86 J versus 1.88 J, and 1.63 J versus 1.59 J). Different results were obtained when the delivered mechanical energy E_L was calculated from P_L. The differences between Tissue resistance model and Airway resistance model were significant for all respiratory rates, up to 20% higher in Tissue resistance model (1.93 J versus 1.60 J, 1.78 J versus 1.57 J, and 1.63 J versus 1.46 J). In contrast, the differences in E_L between Airway resistance and No-resistance models were zero or minimal (1.60 J versus 1.55 J, 1.57 J versus 1.57 J, and 1.46 J versus 1.51 J).

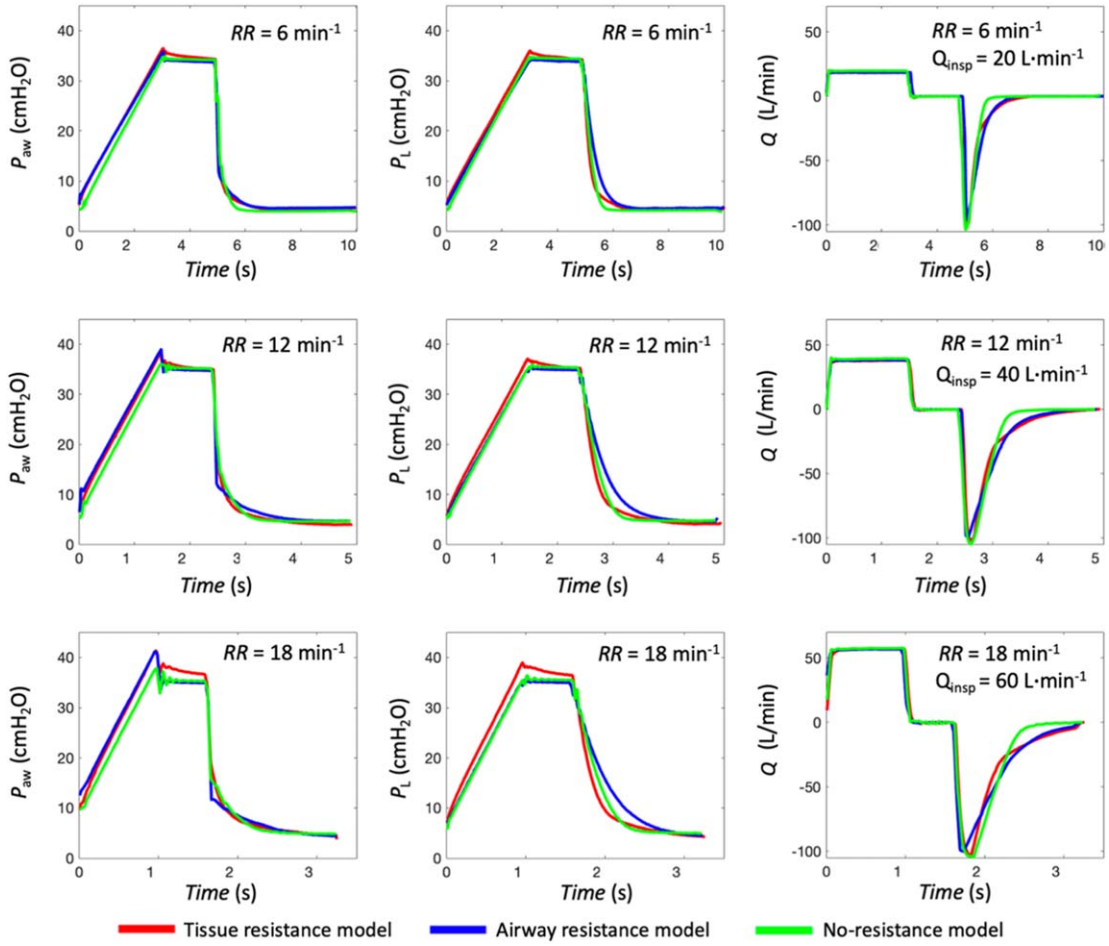

Figure 3. Time dependence of P_{aw}, P_L and Q at respiratory rate settings RR = 6, 12 and 18 min^{-1}, representing Q_{insp} = 20, 40 a 60 l·min^{-1}, for the respiratory system model configurations tested.

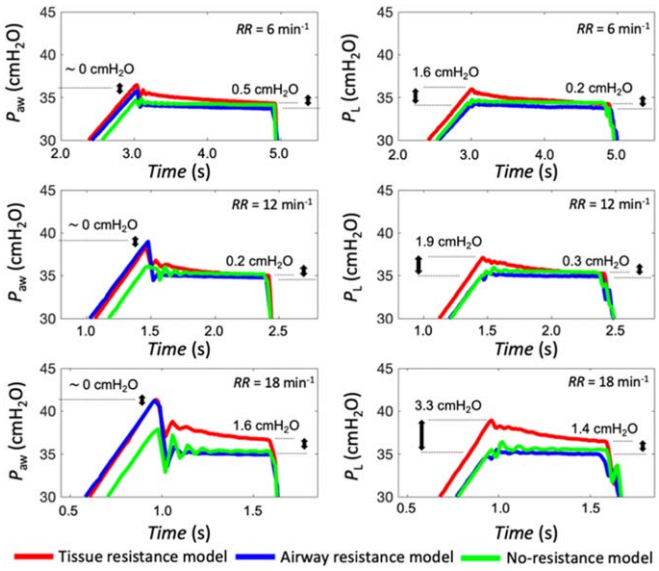

Figure 4. A detailed view of the time courses of P_{aw} and P_L during the inspiratory phase at respiratory rates of 6, 12 and 18 min^{-1} for the tested respiratory system model configurations.

4. Discussion

The main finding of this study is that it is possible to achieve the same time courses of P_{aw} during the inspiratory phase, peak P_{aw} and delivered mechanical energy between Tissue resistance model and Airway resistance model, despite the different origins of the resistances situated at different locations. In contrast,

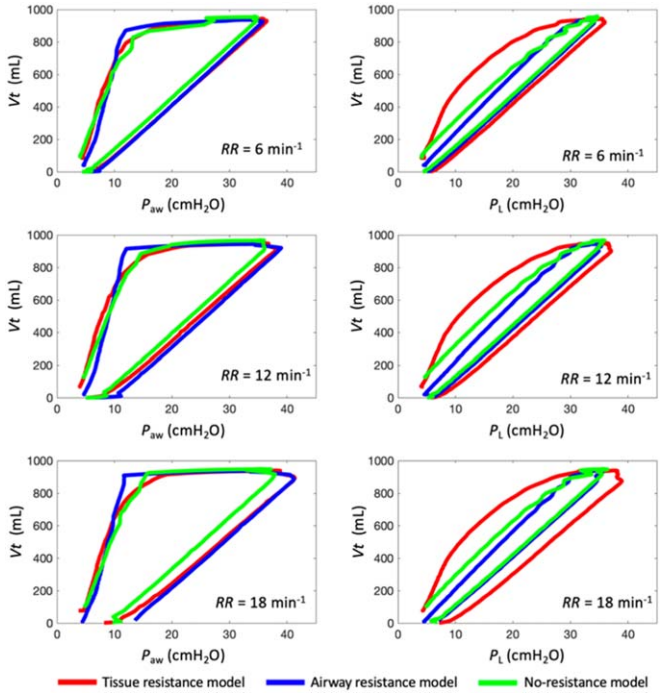

Figure 5. *PV* loops for P_{aw} and P_L during the whole respiratory cycle at respiratory rates 6, 12 and 18 min^{-1} for all the three tested respiratory system model configurations.

Table 1. Mechanical energy delivered (E_{aw}, E_L) to individual respiratory system model configurations at different respiratory rates calculated from measured P_{aw} and P_L.

Respiratory system model configuration	RR (min^{-1})	E_{aw} (J)	E_L (J)
Tissue resistance	18	2.08 ± 0.01	1.93 ± 0.02
	12	1.86 ± 0.02	1.78 ± 0.02
	6	1.63 ± 0.03	1.63 ± 0.03
Airway resistance (5 $cmH_2O \cdot s \cdot L^{-1}$)	18	2.16 ± 0.01	1.60 ± 0.01
	12	1.88 ± 0.03	1.57 ± 0.02
	6	1.59 ± 0.01	1.46 ± 0.01
No-resistance	18	1.81 ± 0.01	1.55 ± 0.02
	12	1.72 ± 0.04	1.57 ± 0.04
	6	1.56 ± 0.04	1.51 ± 0.04

in our physical model of the respiratory system representing only viscoelasticity, when analyzing the delivered mechanical energy calculated from the pressure measured inside the artificial lung, the values in Tissue resistance model were up to 20% higher than those in Airway resistance model.

As the artificial lung of the Simulator inflates, its volume increases, causing the syringe plunger to move and air to pass through the throttle valve in Tissue resistance model. The rapid increase in volume of the artificial lung creates a negative pressure inside the syringe chamber due to the high airflow resistance of the throttle valve. This negative pressure, which reduces the compliance of the artificial lung, is time-dependent on the airflow resistance of the throttle valve and the volume increase in the syringe chamber. During inspiratory occlusion, when the increase in volume of the artificial lung stops, the pressure difference between the syringe chamber and the ambient air exponentially equalizes, while at the same time the pressure inside the artificial lung exponentially decreases.

During the inspiratory occlusion, the pressure decreased by an average of 2 to 3 cmH_2O in Tissue resistance model, depending on the ventilation parameters. This is consistent with the studies conducted by Santini *et al* and Mezidi *et al* where an average decrease of 2 to 3 cmH_2O was observed during a 2 s inspiratory occlusion, depending on the ventilation parameter settings (Mezidi *et al* 2017, Santini *et al* 2019). Pressure differences between the beginning and the end of a 5-s inspiratory occlusion ranged from 2 to 8 cmH_2O depending on Q_{insp} (15–96 $l \cdot min^{-1}$) in a study on piglets (Protti *et al* 2016). Barberis *et al* discovered that measuring P_{plat} immediately at the start of the inspiratory occlusion caused an overestimation of true P_{plat} by 11% in Acute Respiratory Distress Syndrome (ARDS) patients and by 17% in Chronic

Obstructive Pulmonary Disease patients (Barberis *et al* 2003).

Increasing Q_{insp} while keeping all other parameters constant (*Vt*, *PEEP*, *I:E*, C_L) resulted in an increase in peak airway pressures and delivered mechanical energy. However, in No-resistance model, the increase was minimal, likely due to the short narrowing at the airway opening of the artificial lung. Although there was no difference in peak pressures and in the delivered mechanical energy at the airway opening between Tissue resistance and Airway resistance models, a significant difference was observed when calculating the mechanical energy from the pressure measured inside the artificial lung, which is likely crucial for determining the degree of lung ventilation protectivity. The mechanical energy calculated from the measured pressure inside the artificial lung (P_L) was 10% higher at lower Q_{insp} and up to 20% higher at higher Q_{insp} in Tissue resistance model than in Airway resistance model.

Thus, the results of this study indicate that current methods of calculating delivered mechanical power from the measured pressure at the airway opening do not take into account the effect of tissue resistance or the duration of inspiratory occlusion, although parenchymal relaxation and the resulting decrease in pressure during inspiratory occlusion are already known (Ganzert *et al* 2009, Protti *et al* 2016, Santini *et al* 2019). Routine measurements of pressure at the airway opening may underestimate the pressure exerted on the lung parenchyma because a fraction of the measured pressure may be incorrectly attributed to airway resistance. Based on these results, it would be advisable to revise the conditions for using mechanical power delivery calculations, or at least to emphasize the limitations of calculating mechanical power delivery to the lungs.

Assuming only viscoelasticity, revision could consist of introducing a sufficiently long inspiratory occlusion and monitoring the pressure curve at the airway opening during the inspiratory occlusion to separate airway flow resistance from tissue resistance. A 5-s inspiratory occlusion was found to be sufficient to reach the stabilized P_{plat} in the lung parenchyma (Barberis *et al* 2003). Monitoring the course of the pressure curve is particularly important for distinguishing tissue resistance from airway flow resistance, as isolated peak pressure values or isolated P_{plat} values may be the same and thus not allow a complete interpretation of respiratory mechanics. The degree of pressure decrease during this inspiratory occlusion may correlate with subsequent clinical outcomes during mechanical ventilation. For example, in the study by Protti *et al* the level of strain rate, which caused a difference between the measured pressure at the beginning of inspiratory occlusion and at the end of inspiratory occlusion due to viscous resistance, had a significant effect on the prevalence of pulmonary edema (Protti *et al* 2016). This pressure decrease could then be evaluated along with the mechanical power delivery.

Another way to estimate the protectivity of lung ventilation could be to calculate the dissipated mechanical energy, which is defined as the difference between the mechanical energy delivered and the mechanical energy returned (Barnes *et al* 2018). However, this would again require a sufficiently long inspiratory occlusion.

Overall, not being aware of other natural and pathological mechanical properties of the respiratory system, such as tissue resistance, can affect not only the calculation of mechanical power delivered to the lungs, but also, for example, the static compliance shown on the ventilator's display and, subsequently, the clinician's assessment of the patient's condition. In addition, it is always important to be aware of air leaks in the breathing circuit, as these can further affect the resulting values. The use of esophageal pressure monitoring (Piquilloud *et al* 2024) may also be useful in this case, as it is possible to obtain pressure values cleansed of airway resistance. However, the use of an esophageal balloon catheter carries additional complications and significant costs.

While the negative effects of high pressures acting in lung parenchymal tissue are well known, higher pressures acting in the proximal airways may not necessarily be harmful, unless it reflects high pressure in parenchymal tissue. A highly cited study (Amato *et al* 2015) found a relationship between a driving pressure, calculated as a difference between P_{plat} and *PEEP*, and survival rate in ARDS patients. The driving pressure calculation does not consider the effects of pressures acting in the proximal airways, possibly suggesting negligible harmful effects to the proximal airways. On the other hand, high strain rates (velocity) increase stress, causing distortion of epithelial cells in peripheral airways (Pelosi and Rocco 2008, Garcia *et al* 2008) and distal airways (Jain and Sznajder 2007). To summarize, current literature indicates that both airway and tissue pressures need to be monitored and minimized.

The expiratory part of the respiratory cycle was not analyzed in detail in this study. However, we speculate that the developed physical viscoelastic model of the respiratory system could potentially be useful in studies focusing on the analysis of the shape of the expiratory curve and the calculation of expiratory time constants, which are useful, for example, to estimate the compliance and resistance of the respiratory system (Al-Rawas *et al* 2013). However, besides the possible technical uncertainties that expiration may be influenced by the design of the expiratory valve and the ventilator control software, we believe that these approaches to estimate respiratory compliance and resistance are too simplistic and neglect the complexity of lung mechanics.

In this study, we assumed that tissue resistance is only affected by viscoelasticity. In fact, tissue resistance

may also depend on other factors such as poroelasticity (Berger *et al* 2016, Concha and Hurtado 2020), and pressure decrease during inspiratory occlusion may also be affected by airflow through distal airways or chest wall mechanics (Protti *et al* 2016).

5. Conclusion

By connecting the borosilicate syringe with the throttle valve in parallel to the artificial lung of the Simulator, the viscoelastic passive physical model of the respiratory system, simulating tissue resistance, was developed. The resulting values of the peak airway pressures and the delivered mechanical energy were similar in the viscoelastic model with tissue resistance and the model incorporating airway flow resistance, despite the different origins of the resistances situated at different locations. In contrast, when the values of the delivered mechanical energy from the pressure measured inside the artificial lung were analyzed, the values for the model with tissue resistance were up to 20% higher than for the model with airway flow resistance.

Current methods for calculating mechanical power delivery do not distinguish between airway flow resistance and tissue resistance, which can have a significant impact on the evaluation, interpretation and significance of mechanical power delivery in terms of lung ventilation protectivity.

Funding

This work was supported by the Grant Agency of the Czech Technical University in Prague, Grant No. SGS23/198/OHK4/3T/17.

Conflict of interest

The authors declared no potential conflicts of interest with respect to the research, authorship, and/or publication of this article.

Ethical statement

This study did not involve any experiments with human or animal subjects. No ethical approval was required for the completion of this study.

Data availability statement

The data that support the findings of this study are openly available at the following URL/DOI: https://ventilation.fbmi.cvut.cz/data/.

ORCID iDs

Simon Walzel https://orcid.org/0000-0003-1309-9567

References

Al-Rawas N *et al* 2013 Expiratory time constant for determinations of plateau pressure, respiratory system compliance, and total resistance *Critical Care (London, England)* **17** R23

Amato M B P *et al* 2015 Driving pressure and survival in the acute respiratory distress syndrome *New Engl. J. Med.* **372** 747–55

Barberis L, Manno E and Guérin C 2003 Effect of end-inspiratory pause duration on plateau pressure in mechanically ventilated patients *Intensive Care Medicine* **29** 130–4

Barnes T, Van Asseldonk D and Enk D 2018 Minimisation of dissipated energy in the airways during mechanical ventilation by using constant inspiratory and expiratory flows–flow-controlled ventilation (FCV) *Med. Hypotheses* **121** 167–76

Bates J H T 2009 *Lung Mechanics: An inverse Modeling Approach* (Cambridge University Press)

Berger L *et al* 2016 A poroelastic model coupled to a fluid network with applications in lung modelling *International Journal for Numerical Methods in Biomedical Engineering* **32** e02731

Birzle A M and Wall W A 2019 A viscoelastic nonlinear compressible material model of lung parenchyma–experiments and numerical identification *J. Mech. Behav. Biomed. Mater.* **94** 164–75

Chi Y, He H and Long Y 2021 A simple method of mechanical power calculation: using mean airway pressure to replace plateau pressure *J. Clin. Monit. Comput.* **35** 1139–47

Concha F and Hurtado D E 2020 Upscaling the poroelastic behavior of the lung parenchyma: a finite-deformation micromechanical model *J. Mech. Phys. Solids* **145** 104147

Cressoni M *et al* 2016 Mechanical power and development of ventilator-induced lung injury *Anesthesiology* **124** 1100–8

Dai Z *et al* 2015 A model of lung parenchyma stress relaxation using fractional viscoelasticity *Med. Eng. Phys.* **37** 752–8

Escolar J D and Escolar A 2004 Lung histeresis: a morphological view *Histology and Histopathology* **19** 159–66

Ganzert S *et al* 2009 Pressure-dependent stress relaxation in acute respiratory distress syndrome and healthy lungs: an investigation based on a viscoelastic model *Critical Care* **13** 1–10

Garcia C S *et al* 2008 Pulmonary morphofunctional effects of mechanical ventilation with high inspiratory air flow *Critical Care Medicine* **36** 232–9

Gattinoni L *et al* 2016 Ventilator-related causes of lung injury: the mechanical power *Intensive Care Medicine* **42** 1567–75

Gattinoni L *et al* 2017 The future of mechanical ventilation: lessons from the present and the past *Critical Care (London, England)* **21** 183

Giosa L *et al* 2019 Mechanical power at a glance: a simple surrogate for volume-controlled ventilation *Intensive Care Medicine Experimental* **7** 61

Goswami S *et al* 2022 Imaging the local nonlinear viscoelastic properties of soft tissues: initial validation and expected benefits *IEEE Trans. Ultrason. Ferroelectr. Freq. Control* **69.3** 975–87

Guerin C and Richard J C 2007 Measurement of respiratory system resistance during mechanical ventilation *Intensive Care Medicine* **33** 1046–9

Höhne T, Wenzel C and Schumann S 2021 Flow-controlled expiration (FLEX) homogenizes pressure distribution in a four compartment physical model of the respiratory system with chest wall compliance *Physiol. Meas.* **42** 07NT01

Ionescu C M, Segers P and De Keyser R 2009 Mechanical properties of the respiratory system derived from morphologic insight *IEEE Transactions on Bio-Medical Engineering* **56** 949–59

Jain M and Sznajder J I 2007 Bench-to-bedside review: distal airways in acute respiratory distress syndrome *Critical Care (London, England)* **11** 206

Maeda Y *et al* 2004 Effects of peak inspiratory flow on development of ventilator-induced lung injury in rabbits *Anesthesiology* **101** 722–8

Marini J J *et al* 2023 Practical assessment of risk of VILI from ventilating power: a conceptual model *Critical Care (London, England)* **27** 157

Marini J J and Jaber S 2016 Dynamic predictors of VILI risk: beyond the driving pressure *Intensive Care Medicine* **42** 1597–600

Marini J J, Rodriguez R M and Lamb V 1986 Bedside estimation of the inspiratory work of breathing during mechanical ventilation *Chest* **89** 56–63

Mezidi M *et al* 2017 Effect of end-inspiratory plateau pressure duration on driving pressure *Intensive Care Medicine* **43** 587–9

Otis A B *et al* 1956 Mechanical factors in distribution of pulmonary ventilation *J. Appl. Physiol.* **8** 427–43

Pasteka R *et al* 2019 Electro-mechanical lung simulator using polymer and organic human lung equivalents for realistic breathing simulation *Sci. Rep.* **9** 19778

Pelosi P and Rocco P R 2008 Effects of mechanical ventilation on the extracellular matrix *Intensive Care Medicine* **34** 631–9

Piquilloud L, Beitler J R and Beloncle F M 2024 Monitoring esophageal pressure *Intensive Care Medicine* **50** 953–6

Protti A *et al* 2016 Role of strain rate in the pathogenesis of ventilator-induced lung edema *Critical Care Medicine* **44** e838–45

Roth C J *et al* 2017 Computational modelling of the respiratory system: discussion of coupled modelling approaches and two recent extensions *Comput. Meth. Appl. Mech. Eng.* **314** 473–93

Santini A *et al* 2019 Effects of inspiratory flow on lung stress, pendelluft, and ventilation heterogeneity in ARDS: a physiological study *Critical Care (London, England)* **23** 369

Silva P L *et al* 2019 Power to mechanical power to minimize ventilator-induced lung injury? *Intensive Care Medicine Experimental* **7** 38

Similowski T *et al* 1989 Viscoelastic behavior of lung and chest wall in dogs determined by flow interruption *Journal of Applied Physiology (Bethesda, Md.: 1985)* **67** 2219–29

Suki B, Barabási A L and Lutchen K R 1994 Lung tissue viscoelasticity: a mathematical framework and its molecular basis *Journal of Applied Physiology (Bethesda, Md.: 1985)* **76** 2749–59

Wall W A *et al* 2010 Towards a comprehensive computational model for the respiratory system *International Journal for Numerical Methods in Biomedical Engineering* **26** 807–27

Wenzel C *et al* 2020 A linearized expiration flow homogenizes the compartmental pressure distribution in a physical model of the inhomogeneous respiratory system *Physiol. Meas.* **41** 045005